


Distinct neural mechanisms construct classical versus extraclassical inhibitory surrounds in an inhibitory nucleus in the midbrain attention network

Received: 12 March 2020

Accepted: 24 May 2023

Published online: 09 June 2023

 Check for updatesHannah M. Schryver ^{1,2} & Shreesh P. Mysore ^{1,3,4} 

Inhibitory neurons in the midbrain spatial attention network, called isthmi pars magnocellularis (Imc), control stimulus selection by the sensorimotor and attentional hub, the optic tectum (OT). Here, we investigate in the barn owl how classical as well as extraclassical (global) inhibitory surrounds of Imc receptive fields (RFs), fundamental units of Imc computational function, are constructed. We find that focal, reversible blockade of GABAergic input onto Imc neurons disconnects their extraclassical inhibitory surrounds, but leaves intact their classical inhibitory surrounds. Subsequently, with paired recordings and iontophoresis, first at spatially aligned site-pairs in Imc and OT, and then, at mutually distant site-pairs within Imc, we demonstrate that classical inhibitory surrounds of Imc RFs are inherited from OT, but their extraclassical inhibitory surrounds are constructed within Imc. These results reveal key design principles of the midbrain spatial attention circuit and highlight the critical importance of competitive interactions within Imc for its operation.

Animals behave in complex environments and are constantly faced with multiple competing stimuli. Selecting the location with the most “important” or highest priority stimulus to guide behavior at any instant is an essential part of adaptive behavior, and operates upon the foundation of a spatial map of relative stimulus priority^{1–4}. Equally essential is the processing and representation of the stimulus at the selected location. For neurons involved in spatial selection, a core characteristic that impacts both these functions is their spatial receptive field (RF), defined as the subset of the spatial locations that a neuron responds to selectively. The excitatory center and classical inhibitory surround of the RF together control the responses of neurons to a stimulus inside the RF, whereas the extraclassical surround controls the modulation of the neuron’s responses by a competing stimulus outside the RF. Thus, understanding how classical and extraclassical surrounds are constructed is essential for understanding how neurons involved in selection

achieve both competitive selection among multiple competing stimuli as well as the processing and representation of the selected target.

The optic tectum (OT, or superior colliculus, SC, in mammals) is a major sensorimotor hub in the midbrain (Fig. 1A). SC/OT neurons encode space topographically, and are also known to encode a spatial map of relative stimulus priority^{2,5–7}. The SC/OT is required for the control of spatial selection and selective attention when a target is present amidst distracters^{8–10}, with OT neurons signaling the highest priority stimulus among competing stimuli categorically^{11–13}. Notably, these competitive interactions within the OT are controlled by long-range inhibition generated by GABAergic neurons in the nearby isthmi pars magnocellularis (Imc; Fig. 1A, B)¹⁴. Specifically, focal inactivation of Imc neurons abolishes stimulus competition within the OT^{15,16}. Additionally, recent results demonstrate that the signaling of the strongest stimulus by the Imc occurs earlier, and is more categorical

¹Department of Psychological and Brain Sciences, Johns Hopkins University, Baltimore, MD 21218, USA. ²Currently, Allen Institute, Seattle, WA, USA. ³The Solomon H. Snyder Department of Neuroscience, Johns Hopkins School of Medicine, Baltimore, MD 21205, USA. ⁴Kavli Neuroscience Discovery Institute, Johns Hopkins University, Baltimore, MD 21218, USA. ✉ e-mail: mysore@jhu.edu

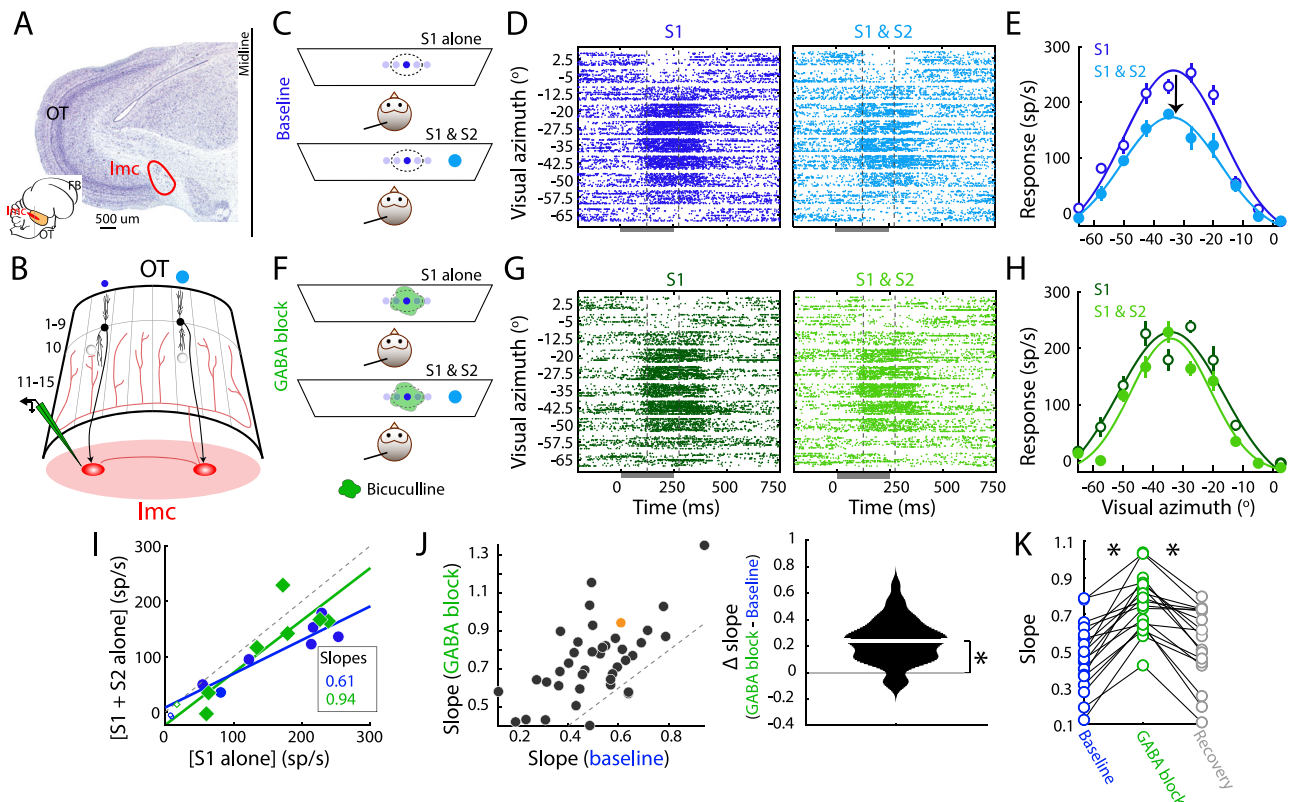


Fig. 1 | Ibc's extraclassical inhibitory surrounds are computed locally in Ibc.

A Inset: Schematic of barn owl brain. OT: optic tectum, Imc: nucleus isthmi pars magnocellularis, FB: forebrain. Vertical line: Coronal section. **Main:** Nissl-stained coronal section. "C"-shaped staining: OT layers. **B** Schematic of Ibc-OT connectivity. Curved sheet: OT; numbers \rightarrow layers (1–15). Columns: topographic encoding of adjacent azimuthal locations¹⁴. Blue dots: stimuli (S1 and S2) at distant azimuths ($>30^\circ$ apart)^{20,27}. Black neurons: OT layer 10 (OT₁₀) neurons encoding these stimuli and providing excitatory input to Ibc neurons (red ovals). Red lines: Inhibitory projections from Ibc neuron on the right to OT intermediate/deep layers (11 to 15; OT_{1d}); projections target OT_{1d} space map broadly sparing only the portion of OT (here, columns) providing input^{14,32}. Horizontal red line: inhibition among Ibc neurons^{26,33}. Projections of left Ibc neuron not shown for clarity. Recording symbol: glass electrode for bicuculline methiodide (green) iontophoresis and recording. **C–E** Baseline condition: Measuring extraclassical (competitive) inhibitory surrounds of Ibc neurons. **C** Stimulus protocol showing owls viewing a monitor, electrode in Ibc (line), RF of Ibc site (dotted oval). Dots: looming stimuli; S1: dark blue, near RF; S2: light blue, distant competitor; dot size: speed of loom (Methods). **D** Raster responses of example Ibc site; dark gray bar: stimulus

duration. RF center: (-31.7° azimuth, -7° elevation); S1 loom speed = $6^\circ/\text{s}$. S2 location: ($+7^\circ$ azimuth, 17° elevation); S2 loom speed = $10^\circ/\text{s}$. Negative azimuths \Rightarrow locations in left hemifield, contralateral to this recording site. Dashed vertical lines: window for firing rate estimation (125–275 ms). **E** Response firing rates (mean \pm s.e.m.). Solid lines: Gaussian fits. **F–H** GABA blockade condition: Same as (C–E), but during focal bicuculline iontophoresis (F, green blob) in Ibc (Methods). **G, H** Responses of Ibc site in D, E during GABA blockade. **I** Scatter plot of responses of the example Ibc site to S1 versus to S1 and S2. Blue: baseline (from E). Green: GABA blockade (from H). Straight lines: Best linear fits to responses at locations within site's RF (large, filled symbols). Slopes: 0.61 (baseline), 0.94 (GABA blockade), $p = 0.044$, one-sided permutation test; smaller values \Rightarrow greater competitive suppression^{20,27}. **J** Population summary. Left: GABA blockade vs. baseline slopes; $n = 40$ sites (after removing 4 outliers; Methods); S2 location = $33.8^\circ \pm 1.03^\circ$ away from Ibc RF center. Orange dot: example site in (D–I). Right: Violin plot of difference in slopes; median = 0.24 (white line). $^{**}p = 8 \times 10^{-8}$, two-sided sign-rank test. **K** Recovery (summary). Slopes at a subset of Ibc sites ($n = 18$) measured in baseline, GABA blockade, and recovery (bicuculline-off) conditions. ** : significant, see text for test and p -values. See also Fig. S1. Source data are provided as a Source Data file.

than in the OT, further highlighting the importance of Ibc to the function of the midbrain selection network.

In turn, Ibc neurons, which have well-defined spatial receptive fields^{17,18}, exhibit both classical inhibitory surrounds and extraclassical competitive surrounds^{18–20}. Specifically, responses of Ibc neurons to a bar stimulus of increasing length (or a circular stimulus of increasing size) have been shown to drop to low values at large lengths (sizes), demonstrating the presence of classical inhibitory surrounds¹⁸. In parallel, responses of Ibc neurons to a stimulus inside the RF are divisively suppressed by a second stimulus anywhere outside the RF, demonstrating a global, extraclassical inhibitory surround. Whereas the source of the excitatory drive for Ibc receptive fields is known to be neurons in layer 10 of the OT (OT₁₀)²¹, how the inhibitory surrounds of Ibc receptive fields are constructed is not understood. Addressing this question is key to understanding how the map of relative stimulus priority is constructed and stimulus selection orchestrated in the OT.

Here, we systematically dissect the mechanisms by which the inhibitory surrounds of Ibc neurons in the barn owl are constructed.

We do so in a series of experiments involving extracellular recordings in the Ibc coupled with iontophoretic silencing of GABAergic input onto Ibc neurons, silencing of GABAergic input onto spatially aligned OT sites, or silencing of excitatory (glutamatergic) input onto other/distant Ibc sites. First, with iontophoretic blockade of GABAergic input on Ibc neurons, we show that whereas global competitive surrounds of Ibc neurons are abolished, the classical inhibitory surrounds are not affected. Then, with paired recording experiments at spatially aligned sites in the Ibc and OT, we demonstrate that classical inhibitory surrounds of Ibc RFs are controlled by inhibition onto OT₁₀ neurons – the sole source of excitatory input to Ibc neurons. Finally, with paired recording experiments at spatially misaligned sites within Ibc, we demonstrate that global competitive surrounds of Ibc RFs are controlled by long-range inhibition from distant Ibc neurons. Our results reveal that distinct mechanisms are involved in the construction of the inhibitory surrounds of Ibc neurons: classical, local inhibitory surrounds are conferred onto Ibc neurons by OT₁₀ neurons, while

global, competitive surrounds are constructed within the lmc using inhibition from distant lmc neurons.

Results

lmc's extraclassical inhibitory surrounds are computed locally in the lmc

We first investigated mechanisms underlying the global, extraclassical inhibitory surrounds exhibited by lmc neurons. Specifically, we asked if the reduction of stimulus-evoked lmc responses by a distant competitor presented outside the RF^{19,20} was due to a comparison occurring at the lmc site itself, or if this response reduction reflected computations occurring elsewhere.

To this end, we conducted extracellular recordings in the lmc using multibarrel glass iontophoresis electrodes filled with a bicuculline methiodide solution (Fig. 1B, Methods). We recorded tuning curve responses at lmc sites using a single stimulus (S1), or while simultaneously also presenting a second, stronger stimulus far outside a site's RF (S2; >30° away; Fig. 1C). Both S1 and S2 were visual looming stimuli whose strengths are controlled by their loom speeds (Mysore et al., 2010; Methods; S1 strength: 6°/s, S2 strength 10°/s). Trials with S1 alone, or S1 and S2 presented simultaneously, were interleaved randomly. Consistent with previous findings, responses to paired S1 and S2 presentations were significantly reduced compared to responses to S1 alone (Fig. 1D, E, I; slope=0.61). We then repeated these measurements following iontophoresis of bicuculline at the lmc recording site (Fig. 1F, Methods), thereby blocking GABAergic synaptic transmission onto the recorded lmc neurons. We found that this nearly abolished the reduction of responses due to the competitor S2, thereby disconnecting this lmc site's extraclassical surround (Fig. 1G–I; slope=0.94; $p = 0.044$, permutation test (GABA blockade vs. baseline slopes)).

Across a population of tested lmc sites ($n = 40$, following the removal of four outliers; Methods), we found that bicuculline iontophoresis at lmc consistently weakened this competitor-dependent response reduction (Fig. 1J, K; $p = 8 \times 10^{-8}$, sign rank test). We verified that these results were specifically due to drug iontophoresis by measuring responses following recovery from bicuculline iontophoresis at a subset of lmc sites ($n = 18$; Methods). We found that competitor-dependent response reduction returned to strong, near-baseline levels (Fig. 1K; baseline vs inactivation, $p = 0.0002$; inactivation vs recovery, $p = 0.0002$; baseline vs recovery, $p = 0.064$; sign rank tests followed by Holm–Bonferroni correction for multiple comparisons). This recovery occurred despite a small, but progressive reduction in the maximum evoked firing rates to S1 alone over time—from the baseline through recovery conditions, consistent with typical time-dependent run-down effects during extended electrophysiological recordings (Fig. S1A–D; Methods).

Together, these results demonstrated that the reduction of lmc responses by a distant competing stimulus is due to suppression caused by GABAergic synapses on these lmc neurons. Global competitive (inhibitory) surrounds are thus constructed locally at the lmc neurons themselves.

lmc's classical inhibitory surrounds are not computed locally in the lmc

We next investigated mechanisms underlying the classical surrounds exhibited by lmc neurons. Specifically, we tested if inhibition impinging onto the neurons, a common mechanism underlying the classical inhibitory surrounds of cortical as well as sub-cortical neurons, mediates the construction of classical surrounds in lmc as well. To this end, we characterized the classical inhibitory surround using a protocol used extensively in the literature, including in lmc—measurement of responses to bar stimuli of systematically increasing lengths (Methods; Fig. 2A)^{18,22,23}. This protocol is well-established to produce response profiles as a function of bar length in which firing rates rise to a peak

before decreasing to an asymptotic value (Fig. S2A)²⁴. This shape of the response profile is the result of the traditional structure of the spatial receptive field—the combination of a strong but spatially narrow excitatory center with a weaker but broader inhibitory surround (Fig. S2B). At small lengths, the excitatory center is activated more than the inhibitory surround, and is activated progressively more as bar length increases, producing the rising phase of response profile. This is followed, at larger bar lengths, by the fixed activation of the spatially limited excitatory center together with an increasing activation of the larger inhibitory surround, producing the falling phase ('dip') of the response profile. Finally, at sufficiently large bar lengths (exceeding the spatial extent of the inhibitory surround), there is fixed activation of both the excitatory center and the surround, producing the asymptotic phase of the response profile (Fig. S2A, B). The shape of the bar length response profile, therefore, reflects the strength and spatial extent of the classical inhibitory surround. Specifically, the amount of suppression of the asymptotic response with respect to the peak response, quantified as the suppression index (SI) = (peak response – asymptotic response)/peak response, is a reliable metric of the classical inhibitory surround, with smaller SI values signaling weaker surrounds^{24,25}.

We measured bar-length response profiles (and SI values; Methods) without and with bicuculline iontophoresis (Fig. 2A) at lmc sites. Within each condition, bars of different lengths were presented in a randomly interleaved manner. Should inhibitory influences onto lmc neurons be involved in creating the classical inhibitory surround, we would expect blockade of this inhibition to substantially alter the bar-length response profile—causing a much smaller dip in responses at medium to large bar lengths and producing a smaller SI value.

We found that the responses of lmc sites to the bar-length protocol exhibited the classic shape (Fig. 2B, C; blue data). However, following bicuculline iontophoresis onto lmc, we found no change in the shape of the bar length response profile, and specifically, no change in the SI (Fig. 2B, C; green data, peak-normalized responses plotted to better visualize any potential changes in shape and SI; SI = 0.58 (baseline, blue), 0.60 (GABA blockade, green), $p = 0.438$; permutation test).

Across a population of lmc sites at which we presented bars of different lengths, we found no systematic effect of bicuculline iontophoresis on SI (Fig. 2D, $p = 0.28$, sign rank test; $n = 28$ sites, following the removal of three outliers; orange dot: example site in B; Methods). Notably, nearly all these sites ($n = 24/28$) were the same as those at which we also obtained the tuning curve data for Fig. 1, with the bar-length response profiles obtained in a randomly interleaved manner with the tuning curve data. We, therefore, were able to rule out the possibility that the drug was ineffective at blocking GABA synapses on lmc neurons in this experiment. Separately, consistent with the results in Fig. S1, we found that the peak evoked responses to bar lengths exhibited a progressive reduction over time, from the baseline through recovery conditions (Fig. S2C–F). Nonetheless, this response run-down did not affect SI, as demonstrated by nearly unchanged SI values across the baseline, GABA blockade and recovery conditions, measured in a subset ($n = 8$) of the sites (Fig. 2E; baseline vs inactivation, $p = 0.38$; inactivation vs recovery, $p = 0.95$; baseline vs recovery, $p = 0.64$; sign rank test followed by Holm–Bonferroni correction for multiple comparisons).

Taken together, these results established that GABAergic inhibition onto lmc neurons does not participate in the construction of their classical inhibitory surrounds.

lmc's classical inhibitory surrounds are inherited from the OT

Since in-situ GABA blockade did not alter the classical inhibitory surrounds of lmc neurons, we next investigated an alternate mechanism for their construction. Specifically, we considered if lmc classical inhibitory surrounds simply reflect the classical inhibitory surrounds

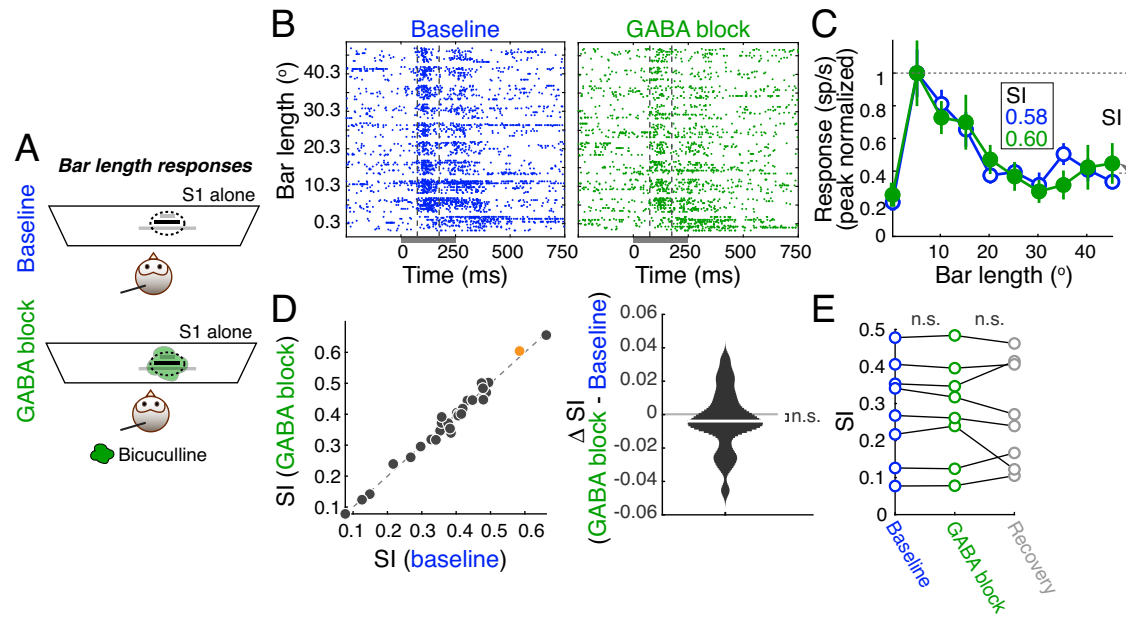


Fig. 2 | Icm's classical inhibitory surrounds are not computed locally in the Icm.

A Bar length protocol for assessing the effect of GABA blockade on Icm classical inhibitory surrounds: a bar stimulus of increasing length was presented inside the spatial RF of the Icm site (dashed oval), in the baseline (Top) and GABA blockade (Bottom) conditions. Bars were horizontal, centered at the azimuthal center of the RF, and had a fixed height of 3° . **B** Raster plots of responses of an example Icm site to bars of increasing lengths in the baseline (Left) and GABA blockade (Right) conditions. RF center of site: (7.53° azimuth, -10° elevation). Positive values of azimuth indicate contralateral locations for this site. Dark gray bar: Stimulus duration (250 ms). Dashed vertical lines: window of responses used for estimating response firing rates (75–175 ms). Other conventions as in Fig. 1D. **C** Firing rate responses (mean \pm s.e.m) as a function of bar length (normalized to peak response),

for site in (B). Blue (open): baseline; green (filled): GABA blockade. Suppression Index (SI) = asymptotic response suppression/peak response (indicated). SI = 0.58 (baseline), and 0.60 (GABA blockade); $p = 0.438$, one-sided permutation test; Methods. **D** Population summary. **Left**: Scatter plot of SI at baseline versus GABA blockade conditions ($n = 28$; after removal of 3 outliers; Methods). Orange dot: example site in (B, C). **Right**: Violin plot of difference between SI values of Icm sites in GABA blockade vs. baseline conditions; median SI value = -0.0039 (white line); 'ns.': not significant; $p = 0.28$, two-sided sign rank test. **E** Recovery (summary). SIs at a subset of Icm sites ($n = 8$), measured in the baseline, GABA blockade, and recovery conditions. 'ns': not statistically significant; two-sided sign rank test, $p < 0.01$, see text for p -values. See also Fig. S2. Source data are provided as a Source Data file.

of the neurons providing excitatory input to them. Neurons in layer 10 of the OT (OT₁₀) provide focal input to Icm neurons, and are the only known source of excitatory drive to them^{14,21}. We, therefore, tested if Icm classical surrounds reflect those of OT₁₀, by performing paired recordings of classical inhibitory surrounds at spatially aligned Icm and OT₁₀ sites, without and with iontophoresis of bicuculline onto OT₁₀ neurons (Fig. 3A; Methods).

To this end, we recorded bar length response profiles at paired Icm-OT₁₀ sites (Fig. 3B). We first examined the effect of OT₁₀ GABA blockade on bar-length response profiles in OT₁₀ (Fig. 3C–F, Methods). At an example OT₁₀ site, following the application of the GABA blockade, we found a significant decrease in the SI (Fig. 3C, D, SI = 0.36 (baseline), 0.04 (OT₁₀ GABA blockade), $p = 0.002$; permutation test), indicating weakening of the classical inhibitory surround in OT₁₀. Across a population of OT₁₀ sites, we found that GABA blockade consistently reduced SI (Fig. 3E, median = -0.18 , $p = 1 \times 10^{-4}$, sign rank test, $n = 14$ sites). Notably, SI values returned to near-baseline following recovery from bicuculline iontophoresis (Fig. 3F, $p = 2 \times 10^{-4}$, baseline vs OT₁₀ GABA blockade; $p = 2 \times 10^{-4}$, OT₁₀ GABA blockade vs recovery; $p = 0.03$, baseline vs recovery, paired sign rank tests corrected for multiple comparisons, $n = 13$ sites at which recovery was also tested). Thus, GABA blockade in OT₁₀ weakened the classical inhibitory surrounds of OT₁₀ neurons.

Next, we examined the effect of this OT₁₀ GABA blockade on bar-length response profiles at paired (spatially aligned) Icm sites (Fig. 3G–J; Methods). At an example Icm site (the Icm site recorded simultaneously with the example OT₁₀ site in Fig. 2C, D, distance between Icm and OT₁₀ RF centers = 1.74°), we also found a significant decrease in the SI value following GABA blockade at the paired OT₁₀ site, indicating weakening of Icm's classical inhibitory surround

(Fig. 3G, H, SI = 0.52 (baseline), 0.15 (aligned OT₁₀ GABA blockade), $p = 0$; permutation test). Across a population of paired (aligned) Icm-OT₁₀ sites, we found that GABA blockade at OT₁₀ consistently reduced SI at Icm sites (Fig. 3I, average distance between Icm and OT₁₀ RF centers = $4.21^\circ \pm 1.32^\circ$; median change in SI = -0.2 , $p = 1 \times 10^{-4}$, sign rank test, $n = 14$ sites). Indeed, SI values returned to near-baseline values following recovery from OT₁₀ bicuculline iontophoresis, demonstrating that the observed effects on SI were due to the drug (Fig. 3J, $p = 2 \times 10^{-4}$, baseline vs OT₁₀ GABA blockade; $p = 2 \times 10^{-4}$, OT₁₀ GABA blockade vs recovery; $p = 0.13$, baseline vs recovery, sign rank tests corrected for multiple comparisons, $n = 13$ sites). Thus, GABA blockade in OT₁₀ also weakened the classical inhibitory surrounds of Icm neurons.

Separately, we found that spontaneous firing rates of OT₁₀ sites increased upon GABA blockade at OT₁₀ and decreased after recovery from the drug (Fig. S3A), consistent with GABA blockade disrupting classical inhibitory surrounds at OT₁₀. Notably, we found that spontaneous firing rates at aligned Icm sites also changed in this way following blockade at OT₁₀: increase after blockade and decrease after recovery (Fig. S3B).

Taken together, these findings established that inhibition onto, and computations at, OT₁₀ are responsible for the expression of classical inhibitory surrounds of Icm neurons, rather than inhibition onto Icm neurons themselves.

Icm's extraclassical inhibitory surrounds are constructed using inhibition from other (distant) Icm neurons

Contrary to classical inhibitory surrounds of Icm neurons, Fig. 1 showed that their extraclassical surrounds are interrupted by blockade of inhibition onto the Icm neurons. We were next interested in identifying the source of this inhibition. Past work in slice has revealed the

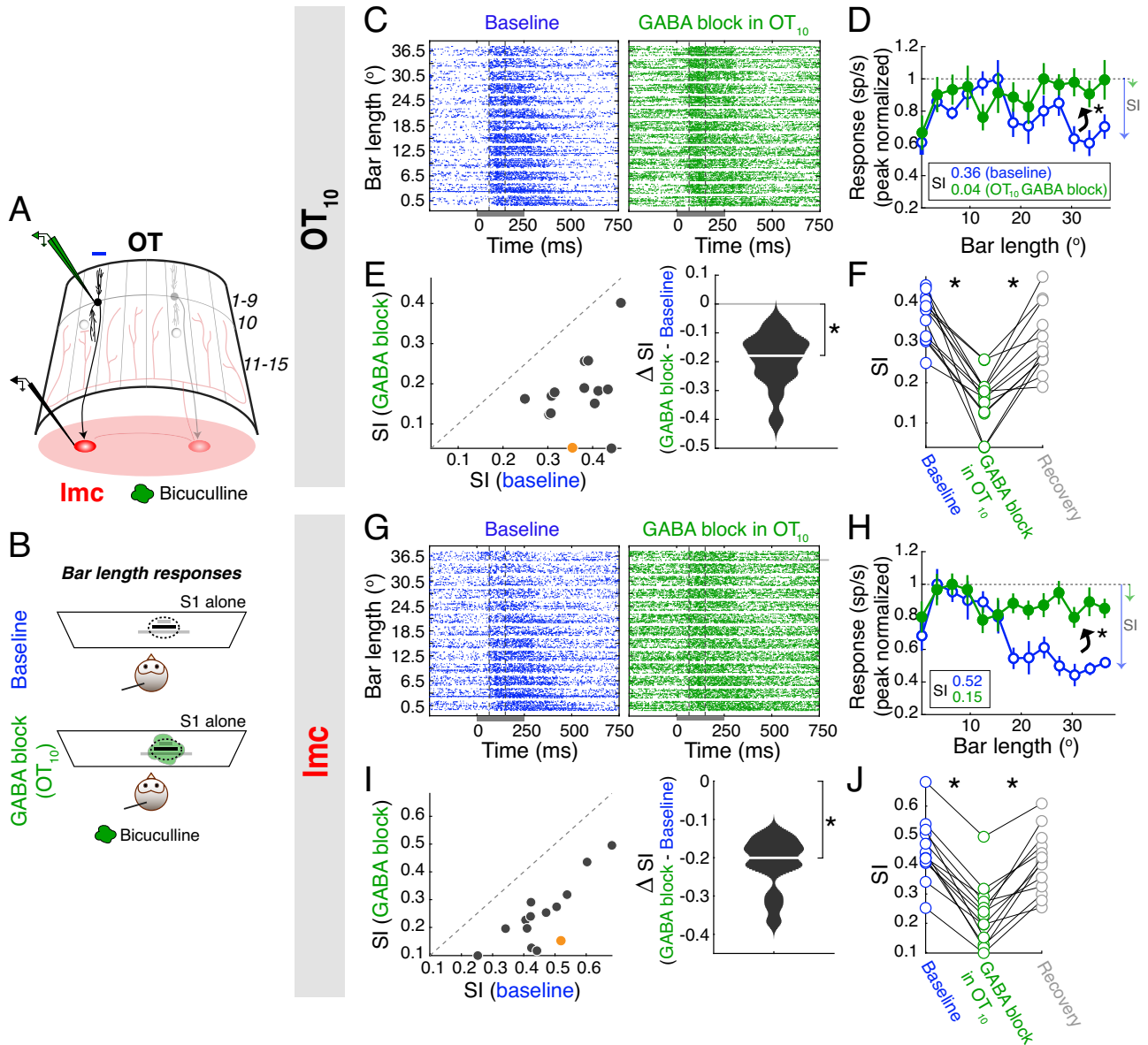


Fig. 3 | Imc's classical inhibitory surrounds are inherited from OT₁₀. **A** Imc-OT schematic showing glass iontophoretic electrode (green, bicuculline methiodide) in OT₁₀, and a second, tungsten electrode (black) at a spatially aligned Imc site; other conventions as in Fig. 1B. **B** Stimulus protocol for measuring bar length response profiles (simultaneously in aligned Imc and OT₁₀ sites) in the baseline condition (Top), and during GABA blockade in OT₁₀ (Bottom); conventions as in Fig. 2A. **C-F** Bar length responses at OT₁₀ sites. **C** Raster plots of responses of example OT₁₀ site. RF center of site = (6.23° azimuth, 10° elevation); positive azimuth values indicate contralateral locations. Dashed vertical lines: 65–150 ms. Conventions as in Fig. 1D. **D** Firing rate responses of site in C (normalized to peak). Blue (open): baseline; green (filled): GABA blockade in OT₁₀. SI = 0.36 (baseline), 0.04 (GABA blockade). **: *p* = 0.002, one-sided permutation test. Other conventions as in Fig. 2C. **E** Population summary (OT₁₀; *n* = 14 sites). Right: Median difference between SI values (OT₁₀) = -0.18 (white line). **: *p* = 1 × 10⁻⁴, two-sided sign

rank test. **F** Recovery (summary). SIs at a subset of OT₁₀ sites (*n* = 13), in baseline, OT₁₀ GABA blockade, and recovery conditions. **: significant; two-sided sign rank test, see text for values. **G-J** Bar length responses at Imc sites that were spatially aligned to the OT₁₀ sites (C-F); conventions as in (C-F). **G** Raster plots of example Imc site (distance of its RF center from OT₁₀ RF center in (C) = 1.74°). **H** Firing rate responses (peak normalized) of site in G. SI = 0.52 (baseline), 0.15 (aligned OT₁₀ GABA blockade). **: *p* = 0, one-sided permutation test. Other conventions as in Fig. 2C. **I** Population summary (Imc); average distance between Imc and OT₁₀ RF centers = 4.21° ± 1.32°. Conventions as in (E). Right: Median difference between SI values (Imc) = -0.2 (white line). **: *p* = 1 × 10⁻⁴, two-sided sign rank test. **J** Recovery (summary). SIs at a subset of Imc sites in baseline, OT₁₀ GABA blockade, and recovery conditions (*n* = 13 Imc sites spatially aligned with OT₁₀ sites from (F)). **: statistically significant; two-sided sign rank test, see text for *p*-values. See also Fig. S3. Source data are provided as a Source Data file.

presence of long-range inhibitory projections between Imc neurons^{14,26}. To test if inhibition from Imc neurons encoding for distant locations controls the construction of extraclassical (competitive) surrounds in Imc, we conducted paired recordings at two mutually distant sites within the Imc (Fig. 4A and S4; Methods). Specifically, using the same stimulus protocol as in Fig. 1 (Fig. 1A, B), we recorded tuning curve responses at one Imc site (site A) using stimulus S1, while

simultaneously presenting S2 at a location > 30° away, encoded by distant Imc neurons with non-overlapping spatial receptive fields (site B; Fig. 4B)^{19,20,27}. We then compared responses at Imc site A without and with iontophoretic silencing of Imc site B using kynurenic acid (Fig. 4B, E; Methods).

We found that in the baseline condition (Fig. 4B), S2 effectively suppressed S1 tuning curve responses recorded at site A (Fig. 4C, D, H;

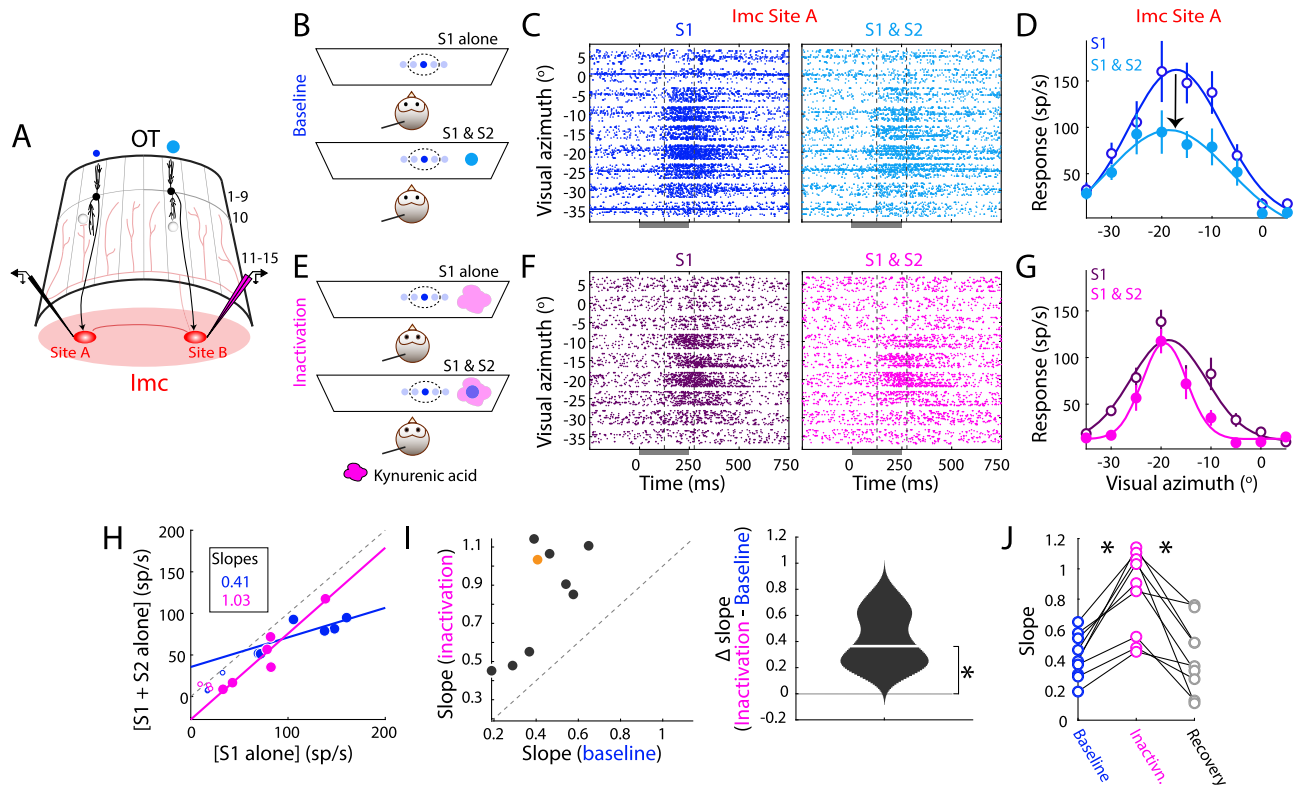


Fig. 4 | Imc's extraclassical inhibitory surrounds are constructed using inhibition from other (distant) Imc neurons. **A** Imc-OT schematic showing a tungsten electrode (black) at Imc site A and a glass iontophoretic electrode (pink, kynurenic acid, for silencing excitatory synaptic drive) at a distant Imc site B. Other conventions as in Fig. 1B. **B–D** Baseline condition: Measuring extraclassical inhibitory surrounds of Imc neurons. **B** Stimulus protocol: Spatial tuning curve at Imc site A without (Top) and with a distant competitor (Bottom; S2 > 30° away from site A's RF center and encoded by Imc site B). **C** Raster responses of example Imc site A. RF center: (−16.41° azimuth, 36° elevation); S1 loom speed = 6°/s. S2 location: (−45° azimuth, 48° elevation); S2 loom speed = 10°/s. Negative azimuths => locations in left hemifield, contralateral to this recording site. Other conventions as in Fig. 1D. **D** Response firing rates (mean ± s.e.m) from (C). Other conventions as in Fig. 1E. **E–G** Imc site B inactivation condition: Same as (B–D), but during kynurenic acid

iontophoresis (E, pink blob) at Imc site B. (F,G) Responses of Imc site A (from panel C) during baseline (purple, filled) and site B inactivation (pink, open) conditions. Distance between site A and site B RF centers = 31°. **G** Response firing rates (mean ± s.e.m) from (F). **H** Scatter plots of responses of the example Imc site A. Blue: baseline (from D). Pink: site B inactivation (from G). Slopes of best fit lines: 0.41 (baseline), 1.03 (site B inactivation), $p = 0.034$, one-sided permutation test. Other conventions as in Fig. 1I. **I** Population summary. **Left**: Site B inactivation vs. baseline slopes ($n = 9$ site pairs); distance between Imc site A and site B RF centers = $44.7^\circ \pm 5.17^\circ$. Orange dot: example site shown in (C–G). **Right**: Violin plot of difference in slopes; median = 0.36 (white line). ***: $p = 0.004$, two-sided sign rank test. **J** Recovery (summary). Slopes ($n = 9$ site pairs), measured in baseline, kynurenic acid, and recovery conditions. **: significant; see text for test and p -values. See also Fig. S4. Source data are provided as a Source Data file.

example site, slope = 0.41). Notably, focally inactivating Imc site B (distant site encoding the competitor stimulus S2; Fig. 4E, Fig. S4A–C), abolished S2's suppressive effect on responses of Imc site A (Fig. 4F–H; slope = 1.03; $p = 0.034$, permutation test of site B inactivation vs. baseline slopes). This effect was consistent across the population of tested site pairs (Fig. 4I-left, $n = 9$ site A-site B pairs): inactivation of Imc site B significantly weakened S2-induced suppression of S1 responses at Imc site A (Fig. 4I-right; median slope increase of 0.36; $p = 0.004$, sign rank test of difference in slopes at site A in baseline vs. site B inactivation conditions).

The observed effects were due, specifically, to drug iontophoresis. First, evoked responses at site B, which were inactivated by kynurenic acid (Fig. S4A, B), returned to near baseline levels following recovery from kynurenic acid (Fig. S4C). Second, S2-induced suppression of S1 responses at site A, which was nearly abolished during kynurenic acid inactivation of site B, also returned to near-baseline levels following recovery (Fig. 4J; $p = 0.004$, baseline vs. site B inactivation; $p = 0.004$, site B inactivation vs. recovery; $p = 0.82$ baseline vs. recovery, paired sign rank tests corrected for multiple comparisons).

We were able to rule out the possibility that the observed effects were due to potential spread of kynurenic acid from Imc site B to Imc site A. We have shown previously that iontophoresis of kynurenic acid at an Imc site does not block evoked responses at distant Imc sites

whose RFs are located more than 25° away¹⁶, and for this reason, in our experiments here, A and B sites were chosen to be much further apart (average distance = $44.7^\circ \pm 5.17^\circ$). To test any effects of potential spread directly, we performed separate experiments in which A and B sites in Imc were similarly far apart (average distance between Imc site A and site B RF centers = $45.7^\circ \pm 6.54^\circ$; $n = 5$; Fig. S4D–F). We confirmed that kynurenic acid iontophoresis at B sites did not spread to A sites: maximum evoked responses at A sites were largely unchanged between baseline and kynurenic acid conditions (Fig. S4D; $p = 0.37$, t-test between peak firing rates; Fig. S4F, site A: $p = 0.63$, Kruskal–Wallis test followed by correction for multiple comparisons), unlike at B sites at which they were suppressed significantly (Fig. S4E; $p = 4 \times 10^{-9}$, t-test between peak firing rates; Fig. S4F, site B: $p = 0.036$, Kruskal–Wallis test followed by correction for multiple comparisons).

Together, these results established that extraclassical inhibitory surrounds of Imc neurons are constructed at the Imc using long-range inhibition from distant Imc neurons, i.e., intra-Imc inhibition is the source of Imc's extraclassical inhibitory surrounds.

Discussion

This study uncovers the mechanistic implementation of classical as well as global inhibitory surrounds of neurons in the Imc, a key mid-brain inhibitory nucleus in the tecto-fugal pathway for visuomotor

(and more generally, sensorimotor) processing in vertebrates⁸. In the parallel thalamo-cortical pathway of visual processing, a related debate on whether the classical surrounds of simple cells in V1²⁸ are constructed within V1 by the action of local inhibitory neurons, or by modulation of excitatory inputs from upstream LGN cells, was only recently resolved²⁹. Selective manipulation of inhibitory neurons within V1 in mice showed that cortical inhibition played a key role in the construction of the classical surround³⁰, thereby establishing a clear mechanism for a basic function of V1 neurons.

In the tecto-fugal pathway, the sensorimotor hub, SC/OT, is not only involved in the processing of individual sensory stimuli, but also plays a critical role in the selection of the highest priority stimulus (target for spatial attention) among competing distracters^{5,6,31}. In turn, neurons in the inhibitory lmc control the competitive interactions within OT^{15,16}. This inhibitory output of lmc neurons reflects computations occurring within lmc rather than being just a sign-flipped version of excitatory inputs into lmc^{19,20}. Indeed, the lmc itself encodes a map of relative stimulus priority^{19,20}, much like the SC/OT – the first reported in inhibitory neurons, to the best of our knowledge. In this context, then, how the responses of lmc neurons to (single and multiple competing) stimuli are constructed, and specifically, how lmc receptive fields are constructed, is a critical, but unanswered, question.

Past work involving recordings in the lmc paired with focal iontophoretic silencing of OT₁₀ neurons have clearly identified OT₁₀ as the source of lmc's excitatory drive²¹. However, although that study also examined the effect of iontophoretic blockade of GABAergic input in lmc on lmc responses²¹, the results are difficult to interpret in the context of the construction of lmc's inhibitory surrounds. In that study, data obtained from the presentation of a single stimulus inside the RF, and from the presentation of two competing stimuli (one inside and one outside the RF), were combined and reported together as a single result. Classical versus global (extraclassical) surrounds have fundamentally different properties in terms of their function, strength profiles, spatial scope, and requirements of the underlying circuitry²⁷. As a result, the properties of one cannot predict those of the other²⁷, highlighting the critical need for considering results from single stimulus versus two-stimulus (competition) protocols separately in order to disambiguate the mechanistic underpinnings of the respective inhibitory surrounds.

Doing so, here, revealed that stimulus competition is computed within the lmc via inhibitory projections among lmc neurons: these long-range projections^{14,26} create global inhibitory surrounds of lmc RFs (Figs. 1, 4). By contrast, classical inhibitory surrounds of lmc RFs are not computed within the lmc (Figs. 2, 3). These latter findings are consistent with the observation in midbrain slice experiments that lmc neurons do not appear to receive projections from nearby (spatially “local”) lmc neurons²⁶. Our results showed, instead, that the classical inhibitory surrounds of lmc RFs are inherited entirely via the excitatory input from OT₁₀ neurons. Indeed, consistent with this finding, we show that spontaneous rates in lmc do increase significantly upon iontophoresis of bicuculline in OT₁₀ (Fig. S3C, D).

An intriguing question that arises from these findings is, ‘why might the lmc-OT circuit be organized this way?’ In other words, why doesn't the lmc inherit both classical and global inhibitory surrounds from the OT, or alternatively, why doesn't it compute both locally? A plausible answer is offered by the fundamental function of the lmc, namely, the orchestration of stimulus selection in the midbrain attention network, and specifically, in the OT.

lmc is the dominant source of competitive inhibition to the intermediate and deep layers of the OT (OTid)^{15,16}, is necessary for the OTid to signal the highest priority stimulus¹⁵, controls selection at all possible pairs of locations in the OTid space map through an optimized combinatorial inhibition solution¹⁷, drives categorical stimulus selection across the OTid space map³², and is thought to be critical for mediating flexibility of selection boundaries in the OT³³. Additionally,

lmc itself expresses signatures of global stimulus competition across space, and does so earlier than the OTid^{19,20}. Consequently, having a dedicated circuit mechanism within the lmc that can implement extraclassical inhibitory surrounds and achieve stimulus competition, would be beneficial.

By contrast, lmc neurons have been shown to not send inhibition to the portion of the OT space map from which they receive input (referred to a donut-like spatial inhibition^{14,32}). Due to this specialized anatomical and functional feature, lmc does not participate in shaping OTid's responses to single stimuli. Consequently, not having a dedicated mechanism within the lmc for generating classical inhibitory surrounds (which typically help shape responses to single stimuli) avoids potentially ‘wasteful’ circuitry that would not aid the core functional role of lmc.

In other words, the computation of global surrounds, but inheritance of classical surrounds, in the lmc may represent an efficient circuit implementation for stimulus selection in the midbrain spatial attention network.

Methods

Experimental design

The goal of this study was to determine the mechanisms underlying the construction of classical and extraclassical inhibitory surrounds of lmc neurons. This was done by measuring (i) spatial tuning curves at lmc neurons using a visual stimulus (S1, presented at various azimuthal locations within and immediately outside the receptive field, RF), (ii) with or without a second visual stimulus present outside of the RF (S2), and separately, measuring (iii) responses to bar stimuli of increasing lengths. All these measurements were made in baseline conditions, and while microiontophoretically applying bicuculline methiodide (Sigma-Aldrich), a GABA_A receptor antagonist locally at the recording site. This allowed us to compare the effect of GABAergic input on local surrounds (S1 tuning curves and bar length response profiles), and as well, on competitive surrounds (S1 tuning curves when S2 was also presented simultaneously).

Additionally, we examined the role of OT₁₀ neurons in the construction of classical inhibitory surrounds of lmc neurons by applying bicuculline methiodide at OT₁₀ sites while simultaneously recording tuning curves and bar length response profiles at both the OT₁₀ site and a paired lmc site encoding for the same area of sensory space (spatially aligned site). Further, to examine the role of lmc neurons in mediating the extraclassical surrounds of other (distant) lmc neurons, we recorded from one lmc site encoding for S1 (site A) without and with S2 presented far outside of the site's RF (>30° away). A second electrode, placed at the distant lmc site encoding for S2 (spatially misaligned site B), was then used to inactivate lmc site B (using kynurenic acid). We compared the responses of lmc sites A in the intact versus site B-inactivated cases. Additionally, in control experiments to assess potential spread of kynurenic acid iontophoresis at site B to site A, we compared the responses of lmc sites A in the intact versus site B-inactivated cases while recording spatial receptive fields at both sites.

Neurophysiology

Eight adult barn owls (*Tyto alba*; no specific sex selection) were used for electrophysiological recordings. All protocols and animal care were in accordance with NIH guidelines for care and use of laboratory animals and approved by the Johns Hopkins University Institutional Animal Care and Use Committee. Birds were shared across different studies and group housed in an aviary with a 12 h/12 h light/dark cycle. Before electrophysiological experiments, head bolts were affixed to the skull under anesthesia (isoflurane, 1–2%, and a mixture of nitrous oxide and oxygen, 45:55). Birds were administered intramuscular injections of 0.1 mL of meloxicam and 0.1 mL of butorphanol, incision areas were disinfected with betadine, and locally anesthetized with

subcutaneously injected bupivacaine. Bilateral craniotomies were performed and small plastic cylinders with removable caps were placed on the skull to allow access to midbrain structures over multiple experiments. Polysporin antibiotic ointment was applied to any exposed brain surface and incisions. Owls were returned to the aviary following recovery from surgery, and experiments were performed starting after a week of recovery.

On experiment days, owls were initially anesthetized with isoflurane (1–2%) and a mixture of nitrous oxide and oxygen (45:55), and administered with intramuscular injections of 0.1 mL of meloxicam and 0.1 mL of butorphanol. Birds were then secured in a sound-attenuating booth, and head-fixation was calibrated for each owl as follows. The pupils were dilated with atropine eye drops, and the pecten structures in the eye were sighted using an ophthalmoscope. The position of the head of the owl was adjusted in roll, pitch and yaw directions such that the pecten structures in the two eyes were positioned symmetrically on either side of the midline (–25 visual degrees from midline), and positioned approximately 7 degrees above horizon³⁴.

Once the bird was calibrated, isoflurane was turned off after the bird was secured, and owls were maintained on oxygen and nitrous oxide for the duration of the experiment. As recovery from isoflurane occurs well under 30 min after it is turned off, recordings were made in animals that were not anesthetized. When possible, nitrous oxide as well was turned off 5 min before data collection (it partitions out of blood rapidly, within a minute). Notably, previous work has demonstrated that neural responses in the midbrain network do not differ under nitrous oxide tranquilization from non-tranquilized conditions¹¹.

The lmc is an oblong structure in the avian midbrain that is elongated along the rostrocaudal axis, parallel to the OT. Previous work has confirmed in vivo targeting of the lmc with fluorescent dye injection¹⁶ and with electrolytic lesions¹⁷, and established its location as approximately 500 μm medial to the medial-most part of the OT. Recording sites in the lmc were targeted by either navigating first to the optic tectum and then to the lmc using the OT's topographic space map as ref. 20, or by referencing reliable stereotaxic coordinates from prior experiments and verified on the basis of established distinct neural responses^{11,16,17,20,27}. For recording in OT₁₀, OT layers were identified by their distinctive neuronal responses³⁴.

Recordings

For lmc recordings, an electrode was positioned to enter the brain at a medial-leading angle of 5° to avoid a major blood vessel. During some paired lmc-lmc recordings, electrodes were additionally angled in the caudal-leading direction (2°–5°) to accommodate space for two electrodes. For paired OT₁₀-lmc recordings, the OT₁₀ targeting electrode was also angled at a 5° medial-leading angle to sterically accommodate both OT₁₀ and lmc electrodes. Extracellular activity in lmc was recorded primarily using multi-barreled glass electrodes with the central barrel containing a carbon fiber electrode for recording neural activity (Kation, Carbostar-3 Carbon fiber electrode). Paired recordings with two electrodes utilized a multi-barreled glass electrode to administer drug and record responses at one brain site, and an epoxy-coated tungsten microelectrode (A-M Systems, 5 M Ω at 1 kHz, 250 μm shaft diameter) to record responses at the paired site. All data in this paper represent a combination of both well-isolated single as well as multi-unit sites. Spike times were recorded using Tucker-Davis hardware and analyzed using MATLAB.

Microiontophoresis

Microiontophoresis was performed using a 1-channel iontophoresis box (DAGAN Corp PS-100). This is an established technique for focal delivery of drugs, and has been used extensively for this purpose in the literature^{32,34}. The drug of interest was filled in one barrel of a multi-

barreled electrode and was microiontophoretically applied to the recording site. Electrophysiological responses were recorded using a carbon fiber electrode in one of the other barrels.

To achieve blockade of inhibitory synaptic input, the GABA_A antagonist bicuculline methiodide (Sigma, 10 mM, 2.37–2.67 pH, mean pH = 2.54) was used. For bicuculline iontophoresis in OT₁₀, we used ejection currents based on published work that has used bicuculline iontophoresis in owl OT (80 nA,^{35,36}. For bicuculline iontophoresis in lmc, we used ejection currents in the range of 20–80 nA (42.5 nA \pm 2.52 nA; n = 44 sites). This was guided by the ranges in published work: 50–100 nA in lmc²¹, 30–120 nA in OT^{35,36}, 20–80 nA in other regions of the central nervous system of several species^{37–41}, and pilot experiments. Bicuculline was ejected at lmc or OT sites for 15 min before data collection in the drug condition and ceased for 25–35 min before data collection in the recovery condition. When not being ejected, bicuculline was retained at a current of –15 nA.

To achieve focal blockade of excitatory synaptic input in lmc, the pan-glutamate receptor antagonist kynurenic acid (Sigma, 40 mM, 8.5–9 pH) was used. For kynurenic acid iontophoresis (in lmc), we used ejection currents established in published work (–500 nA)¹⁶. Kynurenic acid was ejected for 15 min before data collection in the drug condition and ceased for 15 min before data collection in the recovery condition¹⁶. When not being ejected, Kynurenic acid was retained at +15 nA.

Microiontophoretic experiments typically involved three conditions: baseline, drug delivery (GABA or Kynurenic acid) and recovery. By necessity, they are performed serially. The time between the start of “baseline” data collection and the start of “drug” data collection is ~45 min (data collection in each condition takes approximately 30 min, with –15 min wait time in between, for the drug to take effect). Similarly, the time between the start of “drug” data collection and the start of “recovery” data collection is ~45–60 (30 min data collection + –15–30 min wait time for drug's effect to wear off). Such extended electrophysiological recording sessions are known to often result in a progressive run-down of responses over time, which we also observed in our experiments (Figs. S1, S2).

Stimuli

Stimuli were black dots (looming stimuli) or black horizontal bars (stationary stimuli) on a gray background presented on a 65" monitor placed tangentially at a distance of 12.5" in front of the owl. The looming dot stimuli expanded linearly over a duration of 250 ms to mimic approaching objects; previous work has established that looming dot stimuli evoke reliably strong responses in OT and lmc with relatively low response habituation^{11,27}. Bar stimuli were of fixed height (3°), but varying lengths. Stimuli were presented using MATLAB and Psychtoolbox (PTB-3^{42,43}). The spatial locations of visual stimuli were defined by double pole coordinates relative to the midsagittal plane for azimuth or the visual plane for elevation³⁴.

To determine the extent of space encoded by a recorded site (in lmc or OT₁₀), we collected two-dimensional RFs (azimuth \times elevation) by presenting a looming dot stimulus at various azimuthal and elevational locations. Spatial locations at which the stimulus elicited higher firing rates compared to baseline were defined as the site's spatial RF. This was used for determining the placement of S1 (within the RF), of S2 (outside the RF), and for determining the alignment of lmc and OT₁₀ sites.

Tuning curves were measured by presenting S1 of a fixed strength (6°/s) at multiple azimuthal locations spanning the extent of a site's RF. For examining extraclassical surrounds, S2 was presented far outside the RF, at a distant location from S1 (mean distance from RF center = 33.3 \pm 0.91°). S2 loom speed (10°/s), S2 was stronger than of S1. Presentations of S1 alone, and S1 with S2, were interleaved pseudo-randomly. Stimuli were presented for 15 repetitions for collecting the data in Figs. 1–4. For examining classical inhibitory surrounds, bar-length

response functions were obtained by presenting horizontal bars of different lengths (typically, 0.5° to ~40°) centered within the RF. Trials of the three types (tuning curves with S1 alone, tuning curves with S1 in the presence of a distant S2, and bar length response functions) were interleaved randomly. In all cases, stimuli were presented for 15 repetitions, with a duration of 250 ms each and an interstimulus interval of 1500 ms.

Data analysis

All analyses were done with MATLAB scripts. Response firing rates were determined by counting the number of spikes over a time window following stimulus onset and converting this count to firing rate (sp/s) after subtracting the baseline firing rate. This window was chosen to capture well the evoked neural responses: for tuning curves, the count window was from 125 ms to 275 ms with respect to stimulus onset (for I_{mc}¹⁹, and 100 ms to 250 ms (for OT₁₀^{11,26,27,33}). For bar length response curves, the count window was from 65 ms to 175 ms (for both OT₁₀ and I_{mc} sites²⁷). Average rates were calculated across all presentation repetitions.

Statistics

All statistical analyses were performed in MATLAB. Outliers were identified as data points that lay outside the range of median ± 1.5*interquartile range of the distribution. Parametric tests (ANOVA, t-tests) were used if data were normally distributed (tested using a Kolmogorov-Smirnov test, *kstest*), non-parametric tests (Kruskal-Wallis, sign rank) were used otherwise. Correction for multiple comparisons was performed using the Holm-Bonferroni method (for sign rank tests,) and Dunn-Sidak for Kruskal-Wallis, if needed. All tests were two-sided. Data shown as $a \pm b$ refer to mean ± s.e.m, unless specified otherwise. For bar length response functions, the suppression index (SI), was defined as the difference between the peak response and the asymptotic response (estimated as the average response to three widest bars) divided by the peak response.

The permutation test comparing the SI values of bar length response profiles between baseline and GABA blockade conditions (at the example sites in Figs. 2, 3) was performed as follows: First, we randomly assigned firing rates measured at each bar length (15 repetitions × 2 conditions) to either the baseline or GABA blockade condition. Following this, we computed the mean responses (at each bar length), and then the ‘shuffled’ suppression index (‘shuffled’ SI), for each condition, and calculated the difference in shuffled SIs. This procedure was repeated 500 times to generate a distribution of ‘shuffled’ SI differences, and the actual difference in SI was compared to this shuffled null distribution. The p-value was calculated as the proportion of permutations that resulted in a difference greater than or equal to the site’s actual difference of ratios.

The permutation test comparing the slopes of competitive suppression between baseline and GABA blockade conditions (at the example sites in Figs. 1, 4) was performed as follows: First, we randomly assigned firing rate-pairs (for the S1 and S1&S2 presentations) measured at each S1 location (15 repetitions × 2 conditions) to either the baseline or GABA blockade condition. Following this, we computed the mean responses (at each S1 location), and the ‘shuffled’ slope, for each condition, and calculated the difference in shuffled slopes. This procedure was repeated 500 times to generate a distribution of ‘shuffled’ slopes, and the actual difference in slopes was compared to this shuffled null distribution. The p-value was calculated as the proportion of permutations that resulted in a difference greater than or equal to the site’s actual difference of ratios.

For paired I_{mc}-I_{mc} recordings, site-pairs were included only when kynurenic acid iontophoresis caused significant reduction of responses at site B.

Reporting summary

Further information on research design is available in the Nature Portfolio Reporting Summary linked to this article.

Data availability

Data supporting the findings of this study are available in the Zenodo repository⁴⁴: <https://doi.org/10.5281/zenodo.7827183> Source data are provided as a Source Data file. Source data are provided with this paper.

Code availability

The software code that supports the findings of this study are available in the Zenodo repository⁴⁴: <https://doi.org/10.5281/zenodo.7827183>.

References

- Egeth, H. E. & Yantis, S. Visual attention: control, representation, and time course. *Annu. Rev. Psychol.* **48**, 269–297 (1997).
- Fecteau, J. & Munoz, D. Salience, relevance, and firing: a priority map for target selection. *Trends Cogn. Sci.* **10**, 382–390 (2006).
- Knudsen, E. I. Fundamental components of attention. *Annu. Rev. Neurosci.* **30**, 57–78 (2007).
- Koch, C. & Ullman, S. Shifts in selective visual attention: towards the underlying neural circuitry. *Hum. Neurobiol.* **4**, 219–227 (1985).
- Knudsen, E. I. Control from below: the role of a midbrain network in spatial attention. *Eur. J. Neurosci.* **33**, 1961–1972 (2011).
- Krauzlis, R. J., Lovejoy, L. P. & Zénon, A. Superior colliculus and visual spatial attention. *Annu. Rev. Neurosci.* **36**, 165–182 (2013).
- Mysore, S. P. & Knudsen, E. I. The role of a midbrain network in competitive stimulus selection. *Curr. Opin. Neurobiol.* **21**, 653–660 (2011).
- Knudsen, E. I. Neural circuits that mediate selective attention: a comparative perspective. *Trends Neurosci.* **41**, 789–805 (2018).
- Lovejoy, L. P. & Krauzlis, R. J. Inactivation of primate superior colliculus impairs covert selection of signals for perceptual judgments. *Nat. Neurosci.* **13**, 261–266 (2010).
- McPeck, R. M. & Keller, E. L. Deficits in saccade target selection after inactivation of superior colliculus. *Nat. Neurosci.* **7**, 757–763 (2004).
- Mysore, S. P., Asadollahi, A. & Knudsen, E. I. Signaling of the strongest stimulus in the owl optic tectum. *J. Neurosci.* **31**, 5186–5196 (2011).
- Mysore, S. P. & Knudsen, E. I. Flexible categorization of relative stimulus strength by the optic tectum. *J. Neurosci.* **31**, 7745–7752 (2011).
- Mysore, S. P. & Knudsen, E. I. Descending control of neural bias and selectivity in a spatial attention network: Rules and mechanisms. *Neuron* **84**, 214–226 (2014).
- Wang, Y., Major, D. E. & Karten, H. J. Morphology and connections of nucleus isthmi pars magnocellularis in chicks (*Gallus gallus*). *J. Comp. Neurol.* **469**, 275–297 (2004).
- Marín, G. J. et al. A cholinergic gating mechanism controlled by competitive interactions in the optic tectum of the pigeon. *J. Neurosci.* **27**, 8112–8121 (2007).
- Mysore, S. P. & Knudsen, E. I. A shared inhibitory circuit for both exogenous and endogenous control of stimulus selection. *Nat. Neurosci.* **16**, 473–478 (2013).
- Mahajan, N. R. & Mysore, S. P. Combinatorial neural inhibition for stimulus selection across space. *Cell Rep.* **25**, 1158–1170.e9 (2018).
- Wang, Y. C. & Frost, B. J. Visual response characteristics of neurons in the nucleus isthmi magnocellularis and nucleus isthmi parvocellularis of pigeons. *Exp. Brain Res.* **87**, 624–633 (1991).
- Schryver, H. M., Straka, M. & Mysore, S. P. Categorical signaling of the strongest stimulus by an inhibitory midbrain nucleus. *J. Neurosci.* **40**, 4172–4184 (2020).

20. Schryver, H. M. & Mysore, S. P. Spatial dependence of stimulus competition in the avian nucleus isthmi pars magnocellularis. *Brain Behav. Evol.* **93**, 137–151 (2019).
21. Li, D., Xiao, Q. & Wang, S.-R. Feedforward construction of the receptive field and orientation selectivity of visual neurons in the pigeon. *Cereb. Cortex* **17**, 885–893 (2007).
22. Duffy, K. R. & Hubel, D. H. Receptive field properties of neurons in the primary visual cortex under photopic and scotopic lighting conditions. *Vision Res.* **47**, 2569–2574 (2007).
23. Felleman, D. J. & Kaas, J. H. Receptive-field properties of neurons in middle temporal visual area (MT) of owl monkeys. *J. Neurophysiol.* **52**, 488–513 (1984).
24. Sceniak, M. P., Ringach, D. L., Hawken, M. J. & Shapley, R. Contrast's effect on spatial summation by macaque V1 neurons. *Nat. Neurosci.* **2**, 733–739 (1999).
25. Born, G. et al. Corticothalamic feedback sculpts visual spatial integration in mouse thalamus. *Nat. Neurosci.* **24**, 1711–1720 (2021).
26. Goddard, C. A., Mysore, S. P., Bryant, A. S., Huguenard, J. R. & Knudsen, E. I. Spatially reciprocal inhibition of inhibition within a stimulus selection network in the avian midbrain. *PLoS ONE* **9**, e85865 (2014).
27. Mysore, S. P., Asadollahi, A. & Knudsen, E. I. Global inhibition and stimulus competition in the owl optic tectum. *J. Neurosci.* **30**, 1727–1738 (2010).
28. Hubel, D. H. & Wiesel, T. N. Receptive fields of single neurones in the cat's striate cortex. *J. Physiol.* **148**, 574–591 (1959).
29. Alitto, H. J. & Dan, Y. Function of inhibition in visual cortical processing. *Curr. Opin. Neurobiol.* **20**, 340–346 (2010).
30. Zhang, S. et al. Long-range and local circuits for top-down modulation of visual cortex processing. *Science* **345**, 660–665 (2014).
31. Basso, M. A. & May, P. J. Circuits for action and cognition: a view from the superior colliculus. *Annu. Rev. Vis. Sci.* **3**, 197–226 (2017).
32. Mahajan, N. R. & Mysore, S. P. Donut-like organization of inhibition underlies categorical neural responses in the midbrain. *Nat. Commun.* **13**, 1680 (2022).
33. Mysore, S. P. & Knudsen, E. I. Reciprocal inhibition of inhibition: a circuit motif for flexible categorization in stimulus selection. *Neuron* **73**, 193–205 (2012).
34. Knudsen, E. I. Auditory and visual maps of space in the optic tectum of the owl. *J. Neurosci.* **2**, 1177–1194 (1982).
35. Gutfreund, Y., Zheng, W. & Knudsen, E. I. Gated visual input to the central auditory system. *Science* **297**, 1556–1559 (2002).
36. Gutfreund, Y. & Knudsen, E. I. Adaptation in the auditory space map of the barn owl. *J. Neurophysiol.* **96**, 813–825 (2006).
37. Kurt, S., Crook, J. M., Ohl, F. W., Scheich, H. & Schulze, H. Differential effects of iontophoretic in vivo application of the GABA-antagonists bicuculline and gabazine in sensory cortex. *Hear. Res.* **212**, 224–235 (2006).
38. LeBeau, F. E. N., Malmierca, M. S. & Rees, A. Iontophoresis in vivo demonstrates a key role for GABA and glycinergic inhibition in shaping frequency response areas in the inferior colliculus of guinea pig. *J. Neurosci.* **21**, 7303–7312 (2001).
39. McAlpine, D. & Palmer, A. R. Blocking GABAergic inhibition increases sensitivity to sound motion cues in the inferior colliculus. *J. Neurosci.* **22**, 1443–1453 (2002).
40. Toth, L. J., Kim, D. S., Rao, S. C. & Sur, M. Integration of local inputs in visual cortex. *Cereb. Cortex* **7**, 703–710 (1997).
41. Kyriazi, H. T., Carvell, G. E., Brumberg, J. C. & Simons, D. J. Quantitative effects of GABA and bicuculline methiodide on receptive field properties of neurons in real and simulated whisker barrels. *J. Neurophysiol.* **75**, 547–560 (1996).
42. Brainard, D. H. The psychophysics toolbox. *Spat. Vis.* **10**, 433–436 (1997).
43. Pelli, D. G. The VideoToolbox software for visual psychophysics: transforming numbers into movies. *Spat. Vis.* **10**, 437–442 (1997).
44. Schryver, H. M. & Mysore, S. P. Distinct neural mechanisms construct classical versus extraclassical inhibitory surrounds in an inhibitory nucleus in the midbrain attention network. *Zenodo* <https://doi.org/10.5281/zenodo.7827183> (2023).

Acknowledgements

This work was supported by funding from NIH R01 EY027718. We thank Jing Xuan Lim (Department of Neuroscience at Johns Hopkins School of Medicine, and Janelia Farm Research Campus) for performing pilot experiments involving bicuculline iontophoresis in the barn owl Imc.

Author contributions

S.P.M. and H.M.S. designed the research, H.M.S. performed experiments, H.M.S. analyzed the data, S.P.M. and H.M.S. wrote the paper.

Competing interests

The authors declare no competing interests.

Additional information

Supplementary information The online version contains supplementary material available at <https://doi.org/10.1038/s41467-023-39073-5>.

Correspondence and requests for materials should be addressed to Shreesh P. Mysore.

Peer review information *Nature Communications* thanks Yoram Gutfreund, Sam Merlin and the other, anonymous, reviewer(s) for their contribution to the peer review of this work.

Reprints and permissions information is available at <http://www.nature.com/reprints>

Publisher's note Springer Nature remains neutral with regard to jurisdictional claims in published maps and institutional affiliations.

Open Access This article is licensed under a Creative Commons Attribution 4.0 International License, which permits use, sharing, adaptation, distribution and reproduction in any medium or format, as long as you give appropriate credit to the original author(s) and the source, provide a link to the Creative Commons license, and indicate if changes were made. The images or other third party material in this article are included in the article's Creative Commons license, unless indicated otherwise in a credit line to the material. If material is not included in the article's Creative Commons license and your intended use is not permitted by statutory regulation or exceeds the permitted use, you will need to obtain permission directly from the copyright holder. To view a copy of this license, visit <http://creativecommons.org/licenses/by/4.0/>.

© The Author(s) 2023